Hydrogenation Reactions

Deutsche Ausgabe: DOI: 10.1002/ange.201503148
Internationale Ausgabe: DOI: 10.1002/anie.201503148

Pd–Pb Alloy Nanocrystals with Tailored Composition for Semihydrogenation: Taking Advantage of Catalyst Poisoning**

Wenxin Niu, Yongjun Gao, Weiqing Zhang, Ning Yan, and Xianmao Lu**

Abstract: *Metallic nanocrystals (NCs) with well-defined sizes and shapes represent a new family of model systems for establishing structure–function relationships in heterogeneous catalysis. Here in this study, we show that catalyst poisoning can be utilized as an efficient strategy for nanocrystals shape and composition control, as well as a way to tune the catalytic activity of catalysts. Lead species, a well-known poison for noble-metal catalysts, was investigated in the growth of Pd NCs. We discovered that Pb atoms can be incorporated into the lattice of Pd NCs and form Pd–Pb alloy NCs with tunable composition and crystal facets. As model catalysts, the alloy NCs with different compositions showed different selectivity in the semihydrogenation of phenylacetylene. Pd–Pb alloy NCs with better selectivity than that of the commercial Lindlar catalyst were discovered. This study exemplified that the poisoning effect in catalysis can be explored as efficient shape-directing reagents in NC growth, and more importantly, as a strategy to tailor the performance of catalysts with high selectivity.*

Metallic nanocrystals (NCs) have found wide application as heterogeneous catalysts in chemical and energy industries. In heterogeneous catalysis, many significant reactions are highly sensitive to the structure of the catalysts.[1] However, due to the compositional and structural complexity of common catalysts, a comprehensive understanding of the relationship between the catalytic performance and their structures remains a challenging goal.[2] Over the past few decades, the rapid progress in the synthesis of metallic NCs has achieved unprecedented success in controlling their sizes, shapes, and compositions.[3] These research advances offer many degrees of freedom for tuning their catalytic properties.[4] Moreover, the resultant metallic NCs can be a new family of model systems that provide the basis for elucidating structure–function correlations in heterogeneous catalysis.[5] The synergy between fundamental structure–function research in catalysis and new synthetic nanotechnologies will provide the opportunity to design and synthesize highly active, selective, and stable metallic NCs for catalysis.

In catalytic processes, uncontrolled poisoning by exposure to a range of chemical compounds is one of the major mechanisms for the deactivation of precious metal catalysts.[6] Therefore, catalyst poisoning has raised considerable concerns in academic and industrial research. For instance, platinum-based catalytic converters for automobiles can be poisoned if the vehicle is operated on gasoline containing lead additives.[7] However, poisons are not always undesirable. A catalyst can be intentionally poisoned to decrease its activity toward an undesired reaction. A prominent example is the use of lead compounds in the Lindlar catalyst which exhibits high selectivity in the hydrogenation of C≡C to C=C bonds by blocking certain active sites.[8]

The strong interaction of poisoning species with noble-metal catalysts enables a new family of shape-directing reagents for the growth of metal NCs. For example, based on its poisoning effect on Pt and Pd catalysts, carbon monoxide was demonstrated to strongly impact the growth of Pt and Pd NCs.[9] The Lindlar catalyst, a classic example of catalyst poisoning, inspires us that Pb compounds may be utilized as a shape-regulating reagent for the synthesis of Pd NCs. Therefore, in this study, the function of Pb^{II} ions in the growth of Pd NCs was systematically investigated. Unexpected formation of Pd–Pb alloy NCs with tunable shapes and composition was first discovered and explained with a unique alternative deposition mechanism. Moreover, the application of these NCs in the hydrogenation of various alkynes was demonstrated. Pd–Pb alloy NCs with higher selectivity for semihydrogenation of alkynes than the commercial Lindlar catalysts were demonstrated.

The effect of Pb^{II} ions on the growth of Pd NCs was investigated through a seed-mediated growth process. Ascorbic acid (AA) was used to reduce H_2PdCl_4 on Pd cubic seeds in the presence of cetyltrimethylammonium bromide (CTAB). During the reduction process, different amounts of $Pb(NO_3)_2$ solution were introduced to the growth solution. As the concentration of Pb^{2+} increases, the shape of the NCs gradually evolves from cube, to truncated cube, cuboctahedron, truncated octahedron, and octahedron (Figure 1). All these NCs are well-faceted and match well with corresponding geometrical models. With Pb^{II} acetate as the Pb^{II} source, similar shape transition was also observed (Figure S2), suggesting Pb^{2+} is responsible for the shape transition of these NCs.

Transmission electron microscopy (TEM) studies of the cubic, cuboctahedral, and octahedral NCs are shown in Figure 2. Selected-area electron diffraction (SAED) and high-resolution TEM (HRTEM) measurements indicate

[*] Dr. W. X. Niu, Dr. Y. J. Gao, Dr. W. Q. Zhang, Prof. N. Yan, Prof. X. M. Lu
Department of Chemical and Biomolecular Engineering
National University of Singapore
4 Engineering Drive 4, Singapore 117585 (Singapore)
E-mail: ning.yan@nus.edu.sg
xianmao.lu@nus.edu.sg

[**] We thank the Ministry of Education Singapore (Grant no. R279-000-391-112) and the Singapore National Research Foundation (Grant no. R279-000-337-281) for financial support.

Supporting information for this article is available on the WWW under http://dx.doi.org/10.1002/anie.201503148.

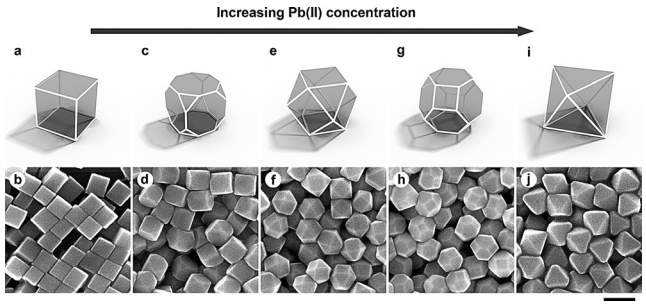

Figure 1. Geometric models and scanning electron microscopy (SEM) images of Pd-based NCs synthesized with different amounts of 10 mM $Pb(NO_3)_2$: a,b) cubes, 0 μL; c,d) truncated cubes, 7 μL; e,f) cuboctahedra, 7.5 μL; g,h) truncated octahedra, 10 μL; i,j) octahedra, 40 μL. Scale bar: 100 nm.

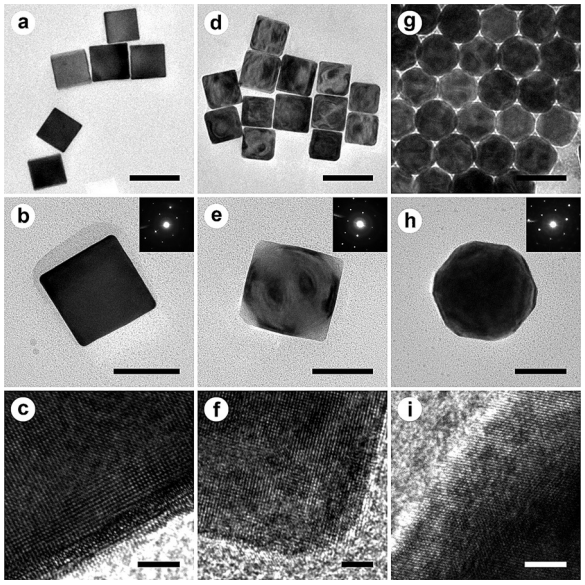

Figure 2. TEM images, SAED patterns, and HRTEM images of Pd-based nanocrystals of three typical shapes : a–c) cubes synthesized in the absence of $Pb(NO_3)_2$, d–f) cuboctahedra synthesized in the presence of 7.5 μL of 10 mM $Pb(NO_3)_2$, g–i) octahedra synthesized in the presence of 40 μL of 10 mM $Pb(NO_3)_2$. Scale bars in (a,d,g) 100 nm, (b,e,h) 50 nm, (c,f,i) 2 nm.

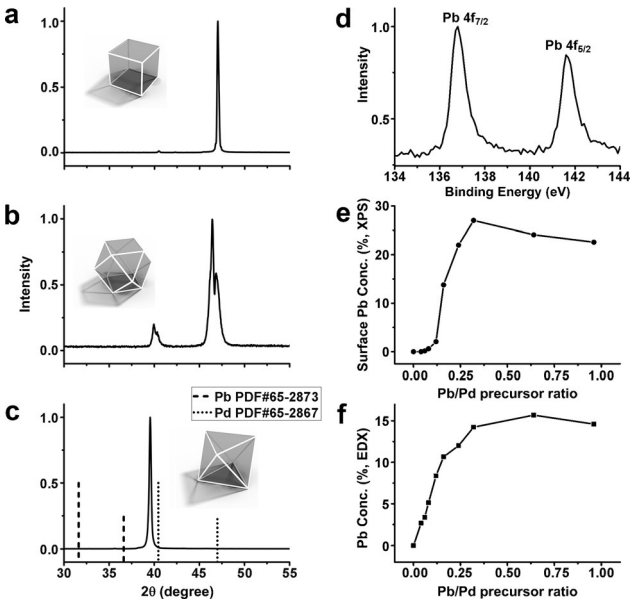

Figure 3. a–c) XRD patterns of cubic, cuboctahedral, and octahedral NCs. d) XPS spectra of Pb 4f region of Pd–Pb alloy NCs, respectively. e) A plot of the surface atomic concentration of Pb (determined by XPS) versus the molar ratio of Pb/Pd precursors. f) A plot of atomic concentration (determined by EDX) of Pb versus the molar ratio of Pb/Pd precursors.

that all the NCs possess a continuous crystal lattice and are highly crystalline. SAED and HRTEM images show that cubic NCs are enclosed by {100} facets (Figure 2a–c). As the volume of Pb^{II} solution increased to 7.5 μL, the corners of the cubes became truncated and the shape of the NCs evolved to cuboctahedra (Figure 2d–f), accompanied by an increased percentage of {111} facet on the surface. When the volume of Pb^{II} solution increased to 40 μL, the final NCs are octahedra mainly enclosed by {111} facets (Figure 2g–i).

The composition of different NCs was determined by X-ray diffraction (XRD), energy-dispersive X-ray (EDX), and X-ray photoelectron spectroscopy (XPS) analyses. The XRD peaks of both the cuboctahedral and octahedral NCs are shifted to lower 2θ values than those of pure Pd nanocubes (Figure 3a–c), suggesting the formation of a Pd–Pb alloy. The ratio between (111) and (200) peak density reflects the abundance of {100} and {111} facets of these NCs, consistent with TEM and SEM results. Interestingly, both (111) and (200) peaks of the cuboctahedral NCs split into two peaks, indicating the Pb atoms are not evenly distributed in the NCs. The XRD pattern of the octahedral NCs show only one (111) peak at a much smaller angle than that of the cuboctahedral NCs.

XPS analysis shows that the surface concentration of Pb on the alloy NCs can be increased to a plateau of 22–27% by increasing the molar ratio of Pb/Pd precursors (Figure 3e). This is close to a stoichiometric Pd_3Pb phase, a stable phase in the Pd–Pb phase diagram.[10] The binding energies of Pb $4f_{7/2}$ and $4f_{5/2}$ core levels are located at 136.8 and 141.6 eV (Figure 3d), corresponding to metallic Pb.[11] EDX analysis shows a similar trend in the overall atomic concentration of Pb, with a plateau at about 15% (Figure 3f). In the region of low molar ratio of Pb/Pd precursors, the overall concentration of Pb increases much faster than the surface concentration of Pb, indicating that at this stage most of the Pb atoms are located in the interior lattice of the NCs. EDX mapping confirmed this assumption (Figure S3).

Tailoring the composition of bimetallic alloy nanostructures provides great flexibility in engineering their properties.[12] However, the synthesis of alloy NCs with well-defined shapes is especially challenging for metals with large potential difference. Therefore, the formation of Pd/Pb alloy NCs with well-defined shapes are quite unexpected because the potential difference between Pb^{2+} and $PdCl_4^{2-}$ ions is over 0.7 V.

To elucidate the mechanism of the formation of Pd–Pb alloy NCs, Pd nanocubes were added to a growth solution containing CTAB, Pb^{II} ions, and AA. Size increase of the Pd nanocubes was not observed after the reaction (Fig-

ure S4a,b), suggesting AA cannot cause the bulk reduction of Pb^{2+}. Nevertheless, XPS studies reveal the existence of metallic Pb on the surface of the nanocubes (Figure S4c), indicating that Pd nanocubes can catalyze the reduction of Pb^{2+} and induce the formation of an ultrathin layer of metallic Pb on the their surfaces. However, such a thin layer of Pb causes the poisoning of the Pd nanocubes NCs and prevents further reduction of Pb^{2+}. The strong interaction of Pd and adsorbed Pb atoms[13] originates from their strong metal–adatom bonding, which is proportional to their large electronegativity difference.[14]

When both $PdCl_4^{2-}$ and Pb^{2+} are involved in the reaction, Pd atoms can still be reduced on the surface of Pb-poisoned NCs due to the high reduction potential of $PdCl_4^{2-}$ ions. After the deposition of Pd atoms, the NCs are able to catalyze the reduction of Pb^{2+} again. Such an alternating Pd- and Pb-deposition process will repeat until the Pb^{II} or Pd^{II} species are depleted. At low concentrations of Pb^{2+}, the Pb atoms were primarily incorporated in the interior crystal lattice of the NCs, closer to the surface of the cubic seeds. Pd atoms confined in the interior of the NCs are beyond the detection depth of XPS techniques, therefore the surface concentration of Pb in the cuboctahedral NCs is extremely low. When the amount of Pb^{2+} increased to the range of 15–40 μL, Pb atoms started to incorporate into the lattice close to the exterior surface of the final NCs and thus the XPS signal increased quickly until a stable Pb surface concentration of 22–27% was reached. During the growth, the deposition of Pb atoms tends to passivate the {111} facets, therefore as the concentration of Pb^{2+} increases, the shapes of the NCs gradually change from cubes with {100} facets to octahedra with {111} facets.

One of the most attracting properties of bimetallic alloy NCs is their highly tunable catalytic properties.[15] The Pd–Pb alloy NCs with tunable compositions are ideal catalysts for establishing their structure–property relationship. Herein, the composition-dependent properties of the Pd–Pb alloy NCs were investigated in the semihydrogenation of phenylacetylene. The catalytic semihydrogenation of alkynes is of special importance in the chemical industries.[16] Although Pd is one of the most widely used catalysts for hydrogenation reactions,[17] Pd usually exhibits low alkene selectivity in alkyne hydrogenation.

Liquid-phase hydrogenation reaction of phenylacetylene was first performed to examine the performance of different Pd–Pb alloy NCs. Six samples of different shapes and surface Pb concentrations were investigated: cubes 0%, cuboctahedra 0.2%, truncated octahedra 2.1%, slightly truncated octahedra 13.8%, octahedra 27.0%, octahedra 0%. The selectivity of different catalysts was shown in Figure 4. For

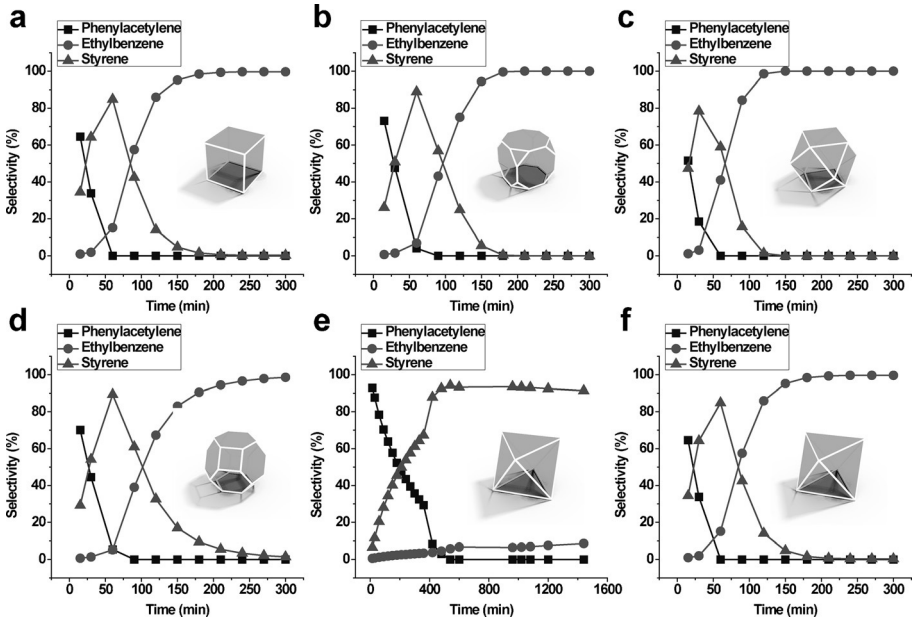

Figure 4. Hydrogenation of phenylacetylene on Pd–Pb NCs of different shapes and Pb surface compositions: a) cubes, 0%; b) cuboctahedra, 0.2%; c) truncated octahedra, 2.1%; d) slightly truncated octahedra, 13.8%; e) octahedra, 27.0%; f) octahedra, 0%.

NCs with low surface Pb concentrations from 0–13.8%, phenylacetylene was first hydrogenated to styrene, which was further hydrogenated to ethylbenzene. In contrast, Pd–Pb alloy octahedral NCs with 27.0% surface Pb dramatically diminished the rate of subsequent hydrogenation of styrene after phenylacetylene was depleted. The semihydrogenation selectivity of Pd–Pb alloy octahedral NCs surpassed the performance of Lindlar catalysts (91.4% vs. 81.1%, Figure S6). Moreover, the Pd–Pb alloy octahedral NCs show even better selectivity at 50°C. After a reaction for 24 h, the Pd–Pb alloy octahedral NCs exhibited a selectivity of 99.1%, whereas the selectivity of the Lindlar catalysts had dropped to only 57.9%. The superior semihydrogenation performance of the Pd–Pb alloy octahedral NCs can be generalized to different alkynes (Table 1).

Table 1: Selective semihydrogenation of alkynes using Pd–Pb alloy octahedral NCs.[a]

Entry	Substrate	*t* [min]	Conv. [%]	Yield [%]	
				Alkane	Alkene
1	2-butyne-1,4-diol	210	96.8	0	96.8
2	1-octyne	210	99.0	13.1	85.9
3	diphenylacetylene	210	96.0	0	96.0
4	1-decyne	210	100	0.6	99.4
5	1-phenyl-1-propyne	300	95.9	2.5	93.4

[a] Reaction conditions: substrate (0.4 mmol) and 0.5 mol% of Pd–Pb alloy octahedral NCs in 2 mL ethanol were stirred at room temperature under 1 atm hydrogen pressure.

The high selectivity of Pd–Pb alloy octahedral NCs in the semihydrogenation process was investigated by Fourier transform infrared spectroscopy (Figure S7). Compared with other Pd and Pd–Pb alloy NCs with lower Pb concentration, the

peaks of adsorbed styrene on Pd–Pb alloy octahedral NCs is neglectable, suggesting that the adsorption of styrene is weakened considerably by Pb alloying. Theoretical studies show that Pb alloying in Pd can strongly shift down the d-band for Pd and induces the reduction of the adsorption energy of molecules with double bonds, whereas a strong binding energy for molecules with triple bonds is still maintained.[18] Improved desorption of styrene with strong adsorption of phenylacetylene is essential to achieve a high selectivity for semihydrogenation. In addition, the addition of Pb can suppress the formation of β-palladium hydride (β-PdH) phase.[18] The presence of β-PdH phase in the Pd catalysts during the hydrogenation reaction is known to considerably increase the acetylene hydrogenation rate to ethane, which is responsible for the low selectivity to ethylene.[19] Moreover, well-defined Pd–Pb alloy NCs possess a uniform distribution of active sites for semihydrogenation. From TEM studies, we can observe that the Pd–Pb alloy NCs have atomically flat crystal facets, thus eliminating the existence of odd active sites and providing a homogenous reactivity over the entire catalysts.[20]

In summary, the poisoning effect of Pb^{II} ions in the synthesis of Pd NCs was first demonstrated. A series of Pd–Pb alloy NCs with tunable shapes and compositions were synthesized, making use of the strong interaction of Pb adatoms and the Pd surface. Moreover, the as-synthesized alloy NCs were applied as model catalysts for the semihydrogenation of alkynes. The Pd–Pb alloy octahedral NCs showed remarkable selectivity for the semihydrogenation of alkynes, which is better than that of the commercial Lindlar catalyst. This study exemplified that the poisons in catalysis can be explored as efficient shape-directing reagents in NC growth and more importantly as a strategy to tailor the performance of catalysts.

Keywords: catalyst poisoning · hydrogenation · Lindlar catalyst · metal nanocrystals · semihydrogenation

How to cite: *Angew. Chem. Int. Ed.* **2015**, *54*, 8271–8274
Angew. Chem. **2015**, *127*, 8389–8392

[1] G. A. Somorjai, J. Y. Park, *Angew. Chem. Int. Ed.* **2008**, *47*, 9212–9228; *Angew. Chem.* **2008**, *120*, 9352–9368.
[2] S. Schauermann, N. Nilius, S. Shaikhutdinov, H.-J. Freund, *Acc. Chem. Res.* **2013**, *46*, 1673–1681.
[3] a) A. R. Tao, S. Habas, P. Yang, *Small* **2008**, *4*, 310–325; b) W. X. Niu, G. B. Xu, *Nano Today* **2011**, *6*, 265–285; c) Y. Xia, Y. Xiong, B. Lim, S. E. Skrabalak, *Angew. Chem. Int. Ed.* **2009**, *48*, 60–103; *Angew. Chem.* **2009**, *121*, 62–108; d) S. Cheong, J. D. Watt, R. D. Tilley, *Nanoscale* **2010**, *2*, 2045–2053.
[4] Y. Li, G. A. Somorjai, *Nano Lett.* **2010**, *10*, 2289–2295.
[5] a) K. An, G. A. Somorjai, *ChemCatChem* **2012**, *4*, 1512–1524; b) F. Zaera, *ChemSusChem* **2013**, *6*, 1797–1820.
[6] C. H. Bartholomew, *Appl. Catal. A* **2001**, *212*, 17–60.
[7] P. Bagot, *Mater. Sci. Technol.* **2004**, *20*, 679–694.
[8] J. G. Ulan, E. Kuo, W. F. Maier, R. S. Rai, G. Thomas, *J. Org. Chem.* **1987**, *52*, 3126–3132.
[9] a) Y. Kang, X. Ye, C. B. Murray, *Angew. Chem. Int. Ed.* **2010**, *49*, 6156–6159; *Angew. Chem.* **2010**, *122*, 6292–6295; b) X. Huang, S. Tang, X. Mu, Y. Dai, G. Chen, Z. Zhou, F. Ruan, Z. Yang, N. Zheng, *Nat. Nanotechnol.* **2011**, *6*, 28–32; c) W. Zhou, J. Wu, H. Yang, *Nano Lett.* **2013**, *13*, 2870–2874.
[10] G. Ghosh, *Metall. Mater. Trans. A* **1999**, *30*, 5–18.
[11] R. B. Shalvoy, G. B. Fisher, P. J. Stiles, *Phys. Rev. B* **1977**, *15*, 1680–1697.
[12] a) J. Gu, Y.-W. Zhang, F. F. Tao, *Chem. Soc. Rev.* **2012**, *41*, 8050–8065; b) W. Zhang, X. Lu, *Nanotechnol. Rev.* **2013**, *2*, 487–514; c) J. Wu, P. Li, Y.-T. F. Pan, S. Warren, X. Yin, H. Yang, *Chem. Soc. Rev.* **2012**, *41*, 8066–8074; d) N. S. Porter, H. Wu, Z. Quan, J. Fang, *Acc. Chem. Res.* **2013**, *46*, 1867–1877.
[13] X.-P. Yan, Z.-M. Ni, *Spectrochim. Acta Part B* **1993**, *48*, 1315–1323.
[14] D. Kolb, M. Przasnyski, H. Gerischer, *J. Electroanal. Chem. Interfacial Electrochem.* **1974**, *54*, 25–38.
[15] a) M. Armbrüster, K. Kovnir, M. Behrens, D. Teschner, Y. Grin, R. Schlögl, *J. Am. Chem. Soc.* **2010**, *132*, 14745–14747; b) Y. Wu, S. Cai, D. Wang, W. He, Y. Li, *J. Am. Chem. Soc.* **2012**, *134*, 8975–8981; c) D. Wang, Y. Li, *Adv. Mater.* **2011**, *23*, 1044–1060.
[16] M. Crespo-Quesada, F. Cárdenas-Lizana, A.-L. Dessimoz, L. Kiwi-Minsker, *ACS Catal.* **2012**, *2*, 1773–1786.
[17] a) H.-U. Blaser, A. Indolese, A. Schnyder, H. Steiner, M. Studer, *J. Mol. Catal. A* **2001**, *173*, 3–18; b) M. Laskar, S. E. Skrabalak, *ACS Catal.* **2014**, *4*, 1120–1128; c) J. Chung, C. Kim, H. Jeong, T. Yu, D. H. Binh, J. Jang, J. Lee, B. M. Kim, B. Lim, *Chem. Asian J.* **2013**, *8*, 919–925; d) R. Long, Z. Rao, K. Mao, Y. Li, C. Zhang, Q. Liu, C. Wang, Z. Y. Li, X. Wu, Y. Xiong, *Angew. Chem. Int. Ed.* **2015**, *54*, 2425–2430; *Angew. Chem.* **2015**, *127*, 2455–2460.
[18] N. Lopez, C. Vargas-Fuentes, *Chem. Commun.* **2012**, *48*, 1379–1391.
[19] a) P. W. Albers, K. Möbus, C. D. Frost, S. F. Parker, *J. Phys. Chem. C* **2011**, *115*, 24485–24493; b) B. Coq, F. Figueras, *J. Mol. Catal. A* **2001**, *173*, 117–134.
[20] M. Crespo-Quesada, A. Yarulin, M. Jin, Y. Xia, L. Kiwi-Minsker, *J. Am. Chem. Soc.* **2011**, *133*, 12787–12794.

Received: April 6, 2015
Published online: May 26, 2015

